

## A MASSIVE, DELAYED EJECTION EVENT IN THE 2011 OUTBURST OF T PYXIDIS

THOMAS NELSON<sup>1</sup>, LAURA CHOMIUK<sup>2,3</sup>, NIRUPAM ROY<sup>3</sup>, J. L. SOKOLOSKI<sup>4</sup>, KOJI MUKAI<sup>5,6</sup>, MIRIAM I. KRAUSS<sup>3</sup>, AMY J. MIODUSZEWSKI<sup>3</sup>, MICHAEL P. RUPEN<sup>3</sup>, & JENNIFER WESTON<sup>4</sup>*Draft version April 11, 2019*

## ABSTRACT

Despite being the prototype of its class, T Pyx is arguably the most unusual and poorly understood recurrent nova. Here, we use radio observations with the VLA to trace the evolution of the ejecta over the course of the 2011 outburst of T Pyx. The radio emission, which is consistent with thermal emission from the nova ejecta, began rising surprisingly late in the outburst, indicating that the bulk of the radio-emitting material was not ejected until  $\sim 50$ – $100$  days after optical discovery. Given that the radio-emitting material must have been ionized, and taking into account the resulting constraints on the electron temperature and clumpiness, the high peak flux densities of the radio emission require a massive ejection of  $[2 - 33] \times 10^{-5} M_{\odot}$ . This ejecta mass is much higher than previous theoretical predictions of outbursts in T Pyx, and implies a very high mass accretion rate onto the white dwarf between outbursts.

*Subject headings:* white dwarfs — novae, cataclysmic variables — stars: individual (T Pyxidis) — radio continuum

## 1. INTRODUCTION

Nova outbursts are the most common stellar explosions in the universe, and are important sources of both energy and matter injection into the ISM (Gehrz et al. 1998). Novae are understood to be the result of a thermonuclear runaway on the surface of an accreting white dwarf (WD). This runaway begins when the critical pressure and temperature required for CNO cycle burning of hydrogen are reached at the base of the accreted shell (Schatzman 1949; Starrfield et al. 1972). As long as accretion continues, all novae are expected to recur on timescales from  $\sim 10^8$  years to less than a year (see e.g. Yaron et al. 2005). This recurrence time depends primarily on the mass of the white dwarf and the accretion rate from the binary companion; more massive white dwarfs have smaller radii and therefore higher surface gravities, meaning that the critical conditions are reached for smaller accreted envelopes. The accretion rate controls the time required to accumulate the critical mass—higher accretion rate systems accrete the trigger mass in less time.

One of the most important predictions of theoretical studies of novae is that most systems experience a net loss in mass during outburst (Yaron et al. 2005), implying severe difficulties in growing WDs to the Chandrasekhar mass so that they explode as SNe Ia. Only white dwarfs accreting material at very high rates from their companions are predicted to eject less mass than had been ac-

creted in the quiescence period prior to outburst (see e.g. Yaron et al. 2005). Such high accretion rates are also expected to result in relatively short intervals between outbursts, with massive white dwarfs experiencing outbursts every decade or so—the observed characteristics of recurrent novae (i.e. the subclass of novae with more than one recorded outburst). Recurrent novae present the best opportunity to determine whether—and in what circumstances—accreting WDs can be SN Ia progenitors, by measuring which is larger: the mass ejected in the nova outburst or the mass accreted since the last outburst. However, the models of Yaron et al. (2005) find that the difference between the accreted and ejected mass is seldom greater than a factor of  $\sim 2$ . Therefore to truly constrain whether a WD is growing or shrinking in mass, we need accurate and precise measurements of both the accretion rate and the ejecta mass. Radio observations are key in determining the latter.

T Pyx is the prototype recurrent nova, with seven outbursts known between 1890 and 1966. However, despite its canonical status and more than a century of study, many questions about this system remain unanswered. T Pyx differs from most other recurrent novae in a number of important ways. The outburst evolution is much slower, taking longer to both rise to maximum light and subsequently fade back to quiescence (Schaefer 2010). T Pyx is the only recurrent nova with an orbital period below the period gap ( $P = 1.83$  h; Schaefer et al. 1992; Patterson et al. 1998; Uthas et al. 2010). Mass transfer in such low period systems is driven by angular momentum loss due to gravitational radiation, which typically leads to accretion rates of order  $10^{-10} M_{\odot} \text{ yr}^{-1}$  or less (Knigge et al. 2011), yet evidence abounds for a high accretion rate in this system (Selvelli et al. 2008). Finally, the binary system is surrounded by a clumpy remnant that is not observed in other recurrent systems, extending up to  $10''$  from the central binary (Williams 1982; Shara et al. 1997; Schaefer et al. 2010).

These unusual characteristics have led to questions about the evolutionary state of T Pyx. The short or-

tnelson@physics.umn.edu

<sup>1</sup> School of Physics and Astronomy, University of Minnesota, 115 Church St SE, Minneapolis, MN 55455<sup>2</sup> Department of Physics and Astronomy, Michigan State University, East Lansing, MI 48824, USA<sup>3</sup> National Radio Astronomy Observatory, P.O. Box 0, Socorro, NM 87801, USA<sup>4</sup> Columbia Astrophysics Laboratory, Columbia University, New York, NY, USA<sup>5</sup> Center for Space Science and Technology, University of Maryland Baltimore County, Baltimore, MD 21250, USA<sup>6</sup> CRESST and X-ray Astrophysics Laboratory, NASA/GSFC, Greenbelt MD 20771 USA

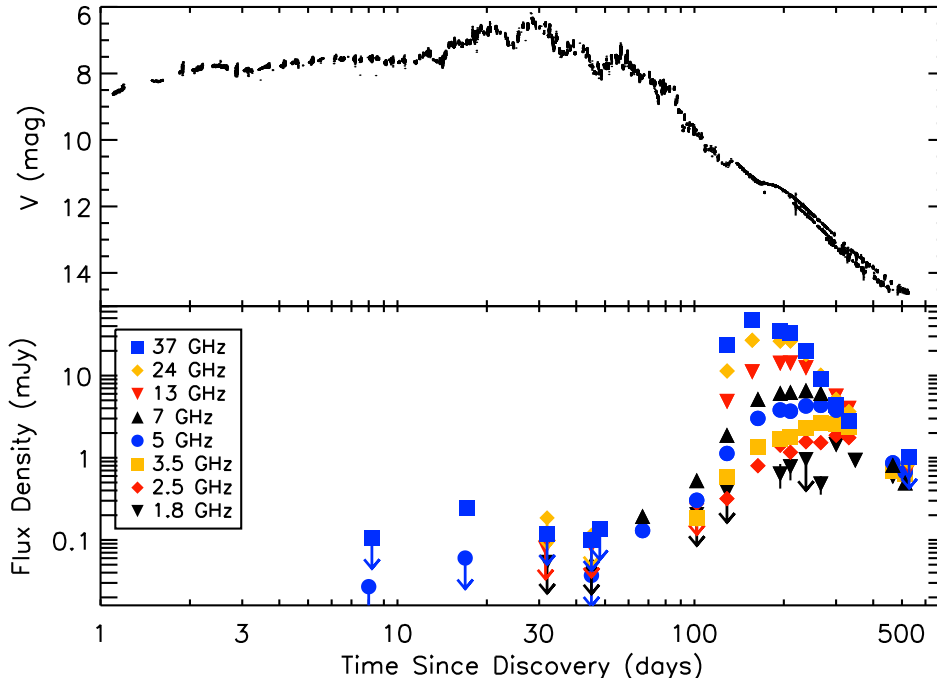


**Figure 1.** Optical and radio light curves of the 2011 T Pyx outburst. Upper panel: V band optical light curve from AAVSO data. Lower panel: VLA light curves at frequencies from 1.5 to 33 GHz. We take 2011 April 14 as  $t_0$ , the start of the outburst.

bitual period and low mass of the companion star make it difficult to maintain the high accretion rate required to power a nova outburst every few decades. To solve this problem, authors have suggested that a normal nova outburst in the late 1800s led to a period of enhanced mass loss induced by irradiation of the companion star by the hot, shell burning white dwarf (e.g., Knigge et al. 2000; Schaefer et al. 2010). This higher mass loss rate in turn fed a higher accretion rate onto the white dwarf, and led to the accumulation of the critical mass required for an outburst in just a decade or so. There is evidence that the average accretion rate between outbursts has been declining over the 20th century, and that the recurrence time between novae has been growing, suggesting that the current state of the T Pyx system is unsustainable for extended periods of time (Schaefer et al. 2010).

T Pyx experienced its most recent outburst in April 2011—the first since 1966, and thus the first eruption for which the astronomical community has been able to obtain broad multiwavelength coverage including the radio regime. The V-band optical light curve of the outburst, created using data from the American Association of Variable Star Observers (AAVSO), is shown in the upper panel of Figure 1. The optical evolution of T Pyx during outburst is much slower and more complex than that observed in most other recurrent novae. The system brightened quickly from its quiescent value of  $V \approx 15.5$  mag to  $V \approx 8$  mag within the first 2 days of outburst. This initial brightening was then followed by a plateau phase, during which the optical brightness remained at  $\sim 8$  mag until around Day 15. T Pyx then began to brighten again, although with some fluctuations, reaching a maximum brightness of  $V \approx 6.5$  mag around Day 30. Over the next two months, the optical light curve declined relatively gradually, with some brightness fluc-

tuations, until around Day  $\sim 90$  at which time the decline suddenly steepened. At the time of completion of this work (October 2012, roughly 1.5 years after the outburst) the V band magnitude as reported by AAVSO observers was  $\sim 14.5$  mag, indicating that the system has not yet fully returned to its quiescence flux levels (Schaefer et al. 2011).

Radio emission in novae traces the bulk of the ejected material in a relatively simple manner—through thermal free-free emission. As the thermal radio emission transitions from optically thick to optically thin and the radio photosphere recedes through the ejecta, the radio light curve surveys the entire density profile of the ejected mass. In this paper we present multifrequency radio light curves of the 2011 nova outburst in T Pyx, obtained with the newly-upgraded Karl G. Jansky Very Large Array (VLA) of the National Radio Astronomy Observatory, and use them to determine the mass of the ejected material. In Section 2, we present our observations and data analysis. In Section 3, we describe the evolution of the radio emission over the course of the outburst. In Section 4, we estimate the mass of the ejecta and the timing of the ejection. Finally, we present our conclusions in Section 6. Throughout this paper, we assume a distance to the system of  $4.8 \pm 0.5$  kpc, derived from light echo observations with the *Hubble Space Telescope* (HST) during the 2011 outburst (Sokoloski et al. 2012, in preparation). This is consistent with the distance of  $>4.5$  kpc inferred from optical spectroscopy by Shore et al. (2011). We also take 2011 April 14.0 UT (MJD = 55665.0) as  $t_0$ , the start of the outburst (Waagan et al. 2011).

## 2. OBSERVATIONS AND DATA REDUCTION

We obtained sensitive radio observations of T Pyx between 2011 April 22 and 2012 September 23 with the

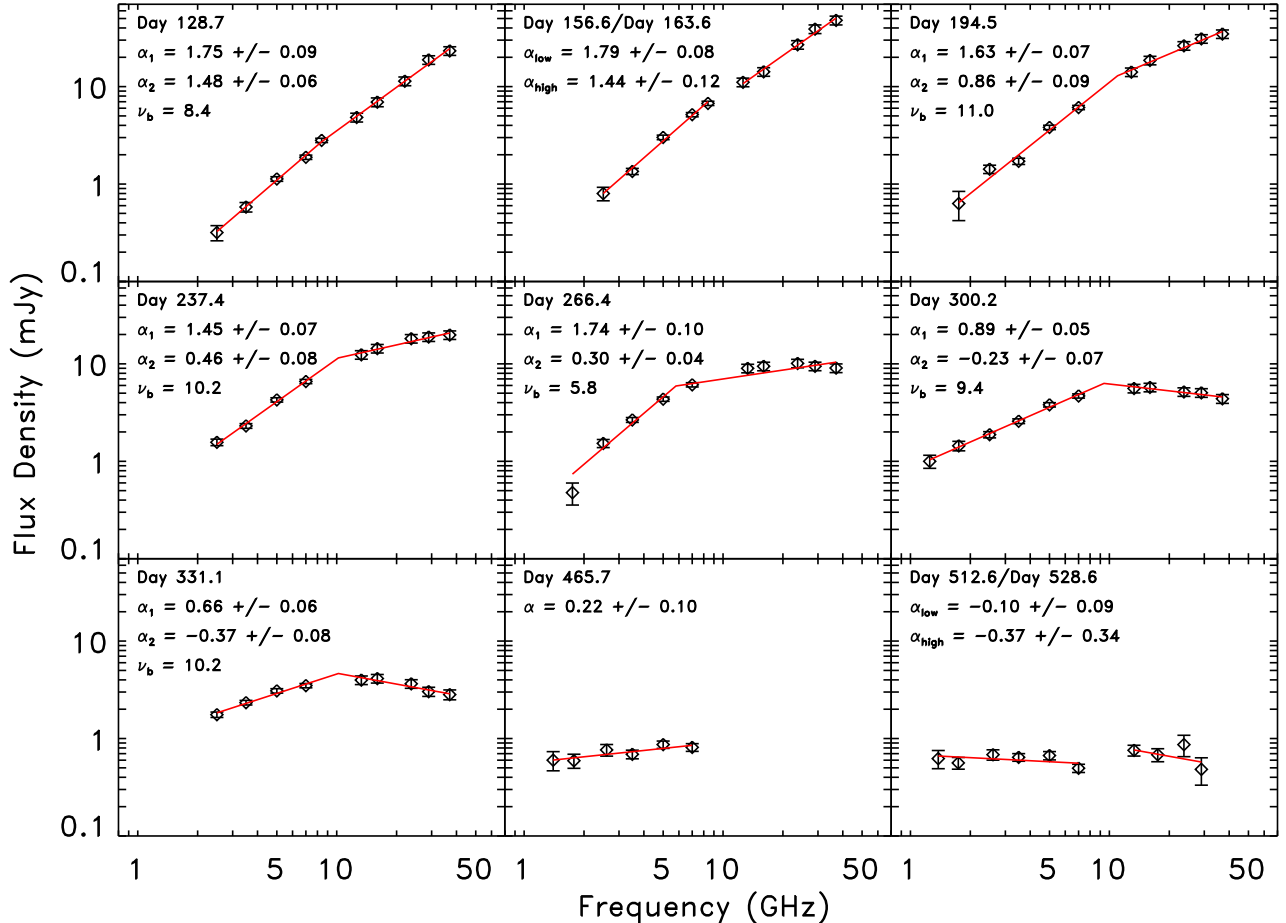


**Figure 2.** A selection of VLA radio spectra over the evolution of the outburst. At each epoch, we over-plot the best-fit single or broken power law spectrum in red. A single index quoted in the top-left corner indicates that a single power law is sufficient to fit the data. Where two indices are quoted,  $\alpha_1$  describes the lower frequency data while  $\alpha_2$  is the fit to the higher frequency data; the break frequency is denoted as  $\nu_b$ . Where low- and high-frequency data are not simultaneous, we fit them separately and report two indices.

VLA through programs 11A-263, 11B-230, and 12A-459. Over the course of the outburst, the VLA was operated in all configurations, and data were obtained in the L (1–2 GHz), S (2–4 GHz), C (4–8 GHz), X (8–8.8 GHz), Ku (12–18 GHz), K (18–26.5 GHz), and Ka (26.5–40 GHz) bands, resulting in coverage from 1–37 GHz. Observations were acquired with 2 GHz of bandwidth (the maximum available), split between two independently tunable 1-GHz-wide basebands, with the exception of L-band observations, which provide 1 GHz of bandwidth between 1–2 GHz, and X-band observations, which were still subject to the old receivers and therefore only cover 800 MHz of bandwidth. The details of our observations are given in Table 1.

At the lower frequencies (L, S, and C bands), the source J0921-2618 was used as the gain calibrator, while J0900-2808 was used for gain calibration at the higher frequencies (X, Ku, K, and Ka bands). The absolute flux density scale and bandpass were calibrated during each run with either 3C138, 3C147, or 3C286. Referenced pointing scans were used at Ku, K, and Ka bands to ensure accurate pointing; pointing solutions were obtained on both the flux calibrator and gain calibrator, and the pointing solution from the gain calibrator was subsequently ap-

plied to our observations of T Pyx. Fast switching was used for high-frequency calibration, with a cycle time of  $\sim 2$  minutes. Data reduction was carried out using standard routines in AIPS and CASA. Each receiver band was edited and calibrated independently. The calibrated data were split into their two basebands and imaged, thereby providing two frequency points, with the exception of X band (where only 800 MHz of bandwidth is obtained, centered at 8.4 GHz) and K band (where the two basebands were placed side-by-side and averaged together). In most cases, when there was sufficient signal, a single iteration of phase-only self-calibration was carried out, with a solution interval of 1–5 minutes, using the clean components from the first imaging run.

One complication affecting our data was that A configuration (the most extended VLA configuration) occurred during the summer months (June–August 2011), when the VLA site is subject to poor weather. These adverse conditions, combined with the low elevation of T Pyx, led to severe decorrelation of many of our A configuration observations, particularly at high frequencies. The K and Ka band data, obtained on 2011 August 20 and September 17, were in particular very badly decorrelated. Despite this problem, significant flux density

was clearly detected; a point source model was used in self-calibration to recover the flux.

In each image, the flux density of T Pyx was measured by fitting a gaussian to the imaged source with the tasks `JMFIT` in AIPS and `gaussfit` in CASA. We record the integrated flux density of the gaussian; in most cases, there was sufficient signal on T Pyx to allow the width of the gaussian to vary slightly, but in cases of low signal-to-noise ratio, the width of the gaussian was kept fixed at the dimensions of the synthesized beam. Errors were estimated by the gaussian fitter, and added in quadrature with estimated calibration errors of 5% at lower frequencies (<10 GHz) and 10% at higher frequencies (>10 GHz). All resulting flux densities and uncertainties are presented in Table 1.

### 3. RADIO EVOLUTION OF THE 2011 OUTBURST OF T PYX

The VLA light curves, presented in the lower panel of Fig 1, show the evolution of the radio emission over the course of the outburst. The source was not detected at either 33 or 6 GHz during the first observation, on Day 8, with upper limits on the flux density  $\leq 0.1$  mJy. Subsequently, on Day 17, T Pyx was detected at 33 GHz at a significance of  $8\sigma$ , but was not detected at 6 GHz. In the next two epochs (Days 31 and 45–48), we observed with additional receiver bands, but the source was not detected at any frequency. The most constraining flux density upper limits at this time were obtained at high frequencies, again with  $F_\nu \leq 0.1$  mJy. On Day 128, observations at 5 and 7 GHz finally resulted in detections of the source at the  $\sim 0.1$  mJy level, and in subsequent observations T Pyx brightened at all frequencies, reaching a maximum flux density of 48 mJy at 37 GHz on Day 156. The radio flux began to fade after this date, first at the highest frequencies, and later at lower frequencies. By Day 538 (the final epoch of observations) the flux density had declined at all frequencies to a level of 0.5–0.9 mJy.

At each epoch, we modeled the resulting spectra as a single power law of the form  $S_\nu \propto \nu^\alpha$  (where  $\alpha$  is the spectral index), and when flux density measurements were obtained at more than 5 frequencies, we also fit a broken power law. The fitting procedure was carried out using `mpfit`, a curve fitting package implemented in IDL (Markwardt 2009). For each spectrum, we compared the goodness of fit of the single and broken power law models, as measured by  $\chi^2/\nu$  (where  $\nu$  is the number of degrees of freedom in the model). We selected the model with the lower value of reduced  $\chi^2$  as the best fit, and plotted it as a red line in each panel of Figure 2. During the early epochs, the broken power law model provides only a marginally better fit to the data than the single power law. However at later times, where the turnover at higher frequencies is quite clear, the broken power law provides a large improvement in the goodness of the fit.

The best fit spectral indices at each epoch indicate an evolution from optically thick emission during the rising phase, to optically thin emission at late times. We present a selection of spectra that best demonstrates this evolution in Figure 2. The spectral indices fit to both the low- and high-frequency data are initially steeply rising ( $\alpha_1 = 1.75 \pm 0.09$ ,  $\alpha_2 = 1.48 \pm 0.06$  on Day 129), indicative of optically thick emission. We note that spec-

tral index implied by the data on Day 17 ( $\alpha \geq 1.14$ ) is also steep, and suggests that the source was also optically thick at the time of first detection. As the outburst evolves the spectrum becomes shallower, beginning first at high frequencies on Day 194, and eventually at low frequencies by Day 300. The best fit indices at high frequencies are between  $\alpha = 0.3$  and 0.8, consistent with the values expected for a partially optically thick shell with a density profile that decreases in the outward direction. By Day 300, the high frequency spectrum has turned over ( $\alpha = -0.23 \pm 0.07$ ), consistent with emission from a completely optically thin shell. By the epochs of our last observations (Days 512 and 528), the spectra have indices expected for optically thin gas at all frequencies.

### 4. EJECTA MASS AND EJECTION TIMING

The radio light curves, and the evolution of the radio spectra from optically thick to thin, are consistent with thermal emission from the expanding nova ejecta. Consider an ionized shell of material, ejected from the surface of the white dwarf shortly after the onset of the nova outburst. The shell is a source of radio flux due to thermal free-free emission. At early times the shell is compact and dense, and is optically thick at all radio frequencies. This yields a steeply rising spectrum with  $\alpha = 2$ , as expected for the Rayleigh-Jeans tail of a blackbody. At this stage, the radio photosphere (i.e. the surface where optical depth  $\tau = 1$ ) at all frequencies is essentially coincident with the outer surface of the ejecta, and increases in surface area as the ejecta expand. This leads to a brightening of the radio emission, and accounts for the rising, steep spectrum portion of the radio light curve.

Some time later, the density in the shell drops sufficiently that the ejecta start to become optically thin. This process begins at high frequencies first, since higher radio frequencies require larger emission measures to be optically thick compared to lower frequencies. The radio photosphere at such a frequency will recede through the ejecta, tracing slower moving ejecta as it goes. This leads to a gradual turnover in the radio light curve, and a flattening of the spectral index (to  $\alpha \approx 0.6$  for an  $r^{-2}$  density profile). This process cascades towards lower and lower frequencies as time passes. Once the photospheres of all observed frequencies have completely receded through the entire ejected shell, the emission can be described completely by optically-thin thermal bremsstrahlung ( $\alpha = -0.1$ ). After this, the radio light curve simply fades at all frequencies as the ejecta expand and the emission measure continues to drop.

We can estimate the mass of the ejecta using simple models that account for the observed radio flux evolution at all frequencies in a consistent manner. Following the work of Seaquist & Palimaka (e.g., 1977); Hjellming et al. (e.g., 1979), we assume that the ejecta can be described as a thick shell of warm ( $T \approx 10^4$  K) material emitting thermal bremsstrahlung radiation. In this model, the shell is ejected at  $t_0$ , i.e. the start of the nova outburst. The density profile of the shell varies with radial distance such that  $\rho(r) \propto r^{-2}$  or  $r^{-3}$ , with an inner boundary to the ejecta. The thickness of the ejected shell may be due to either a velocity spread in a homologous explosion (a Hubble flow) or a prolonged period of mass loss (Seaquist & Bode 2008). The model traces the evolution of the photosphere at each frequency as

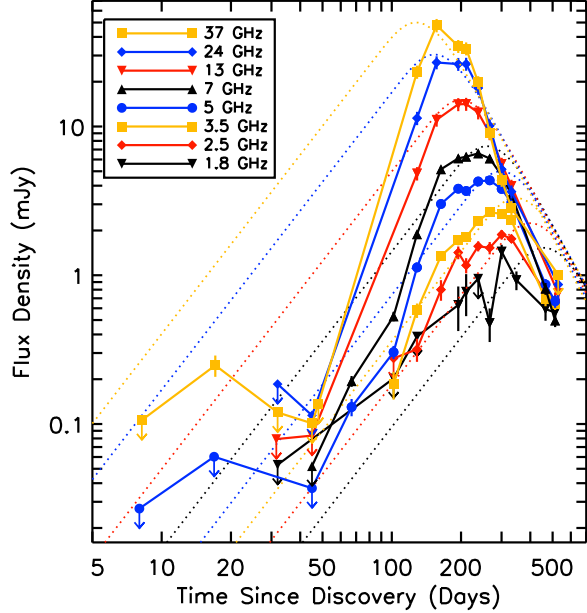


**Figure 3.** Hubble flow model for the radio emission from the nova ejecta, assuming mass ejection at the time of optical discovery. We assume a distance to T Pyx of 4.8 kpc, and expansion velocity of  $3,000 \text{ km s}^{-1}$ . The model plotted here has ejected mass of  $2.5 \times 10^{-4} M_{\odot}$ ,  $T_e = 10,000 \text{ K}$ , and  $v_{\min}/v_{\max} = 0.9$ . The match to the high flux densities observed at peak brightness is relatively, but the model fails to reproduce all other features of the radio evolution.

the ejecta expand over time, and depends on the ejected mass ( $M_{\text{ej}}$ ), the velocity of the outermost ejecta ( $v_{\max}$ ), the electron temperature of the ejecta ( $T_e$ ; assumed to be constant in time and throughout the ejecta), and the distance to the nova ( $d$ ). The turn-over in the light curves also depends on the assumed density profile (we take  $\rho(r) \propto r^{-2}$  here) and on the thickness of the shell, which we parameterize here as the ratio of the velocities in the innermost and outermost ejecta ( $v_{\min}/v_{\max}$ ), assuming an instantaneous and homologous explosion. We fit this model of expanding thermal ejecta to all observed frequencies simultaneously with the singular exclusion of the lower baseband in L band ( $\sim 1.3 \text{ GHz}$ ; this frequency mostly yields non-detections), making use of the `mpfit` package developed for IDL (Markwardt 2009) to carry out least-squares fitting and obtain the best-fit parameters. Measurements that are not significant at the  $3\sigma$  level are excluded from our model fits.

The large flux densities reached at peak radio brightness around Day 200 place important constraints on the mass of the ejected shell. Assuming a distance to T Pyx of  $4.8 \pm 0.5 \text{ kpc}$  (Sokoloski et al. 2012, in preparation), a shell temperature  $T_e$  of  $10,000 \text{ K}$ , and a maximum velocity of the ejecta of  $3,000 \text{ km s}^{-1}$  (the value reported around the time the radio flux begins to rise by Osborne et al. (2011)), we find that only models with  $M_{\text{ej}} \approx 2.5 \times 10^{-4} M_{\odot}$  can reproduce the peak flux densities. An example of such a model is shown in Figure 3. Irrespective of the quality of the fits at early and late times, the requirement that the ejecta must be large and optically thick to produce the high observed radio flux

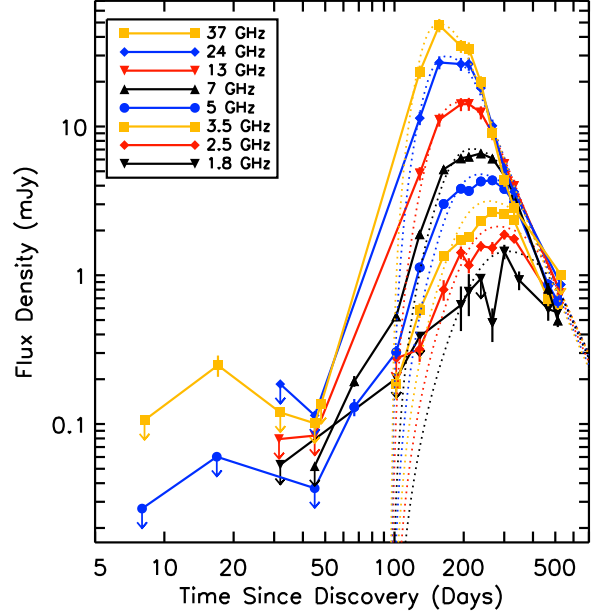


**Figure 4.** Same as Figure 3, but allowing the time of mass ejection to be an additional free parameter. The formal best fit model has  $t_{\text{ej}} = 96 \text{ days}$ ,  $M_{\text{ej}} = 2.2 \times 10^{-4} M_{\odot}$ , and  $T_e = 67,000 \text{ K}$ , and  $v_{\min}/v_{\max} = 0.2$ , although we note that the uncertainties on the ejection date are large.

densities indicates that the density in the ejecta, and hence the mass, must be high.

#### 4.1. Modeling a Delayed Ejection

The rise of the radio flux is not consistent with the primary ejection of material at  $t_0$ . At early times while the ejecta are optically thick, flux densities are expected to rise as approximately  $t^2$  as the ejecta expand. If the material responsible for the radio emission had started expanding at  $t_0$ , we would have detected brightening radio emission at early times (see Figure 3). Our sensitive upper limits rule this out. Despite successfully reproducing the high-frequency peak flux densities, the model shown in Figure 3 fails to reproduce all other details of the observed light curve—the rise of the radio flux, the spectral evolution, and the late decline phase. The observed radio rise is steeper, and begins later in the outburst. Although there is a significant detection of flux on Day 16, the source is faint ( $0.248 \text{ mJy}$  at  $33 \text{ GHz}$ ) and is subsequently undetected at the same frequency in the following two epochs. This early detection detection may be related to some early period of mass loss (see Section 5.3), but it is clearly not related to the primary mass ejection traced by the bulk of the radio emission. This begins much later, starting with the detections at 5 and  $7 \text{ GHz}$  on Day 66.

We obtain much better model fits to the data if we do not require mass to be ejected at the time of optical discovery, and instead allow for a delayed mass ejection. Including the time of ejection (measured relative to the date of discovery, 2011 April 14) as an additional free parameter, we find that the best fit models are those in which the nova shell is ejected between 50 and 100 days after optical discovery. An example fit, in which

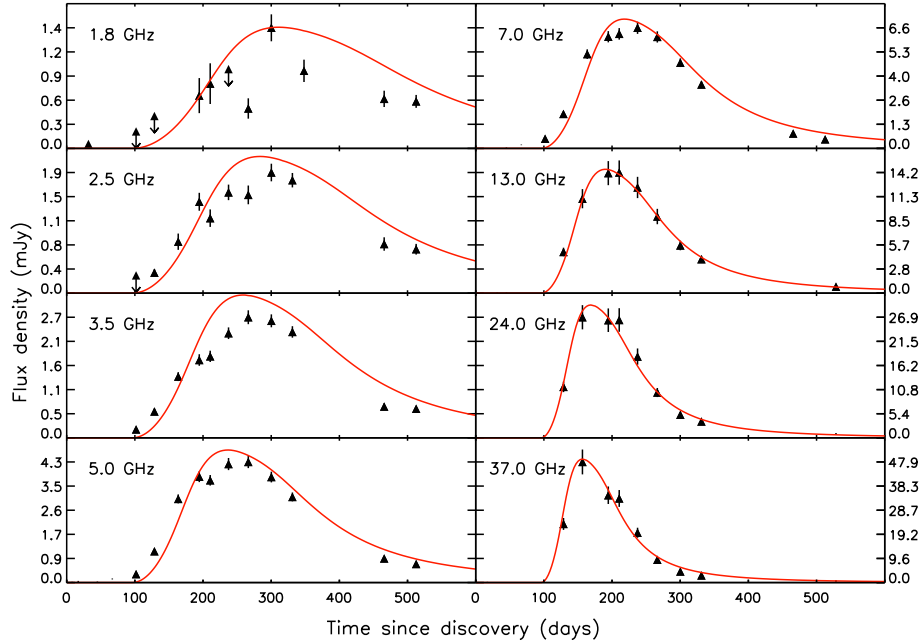


**Figure 5.** VLA light curves of T Pyx, with each frequency occupying its own panel. Red lines represent the model plotted in Figure 4 and discussed in Section 4.1.

we continue to assume  $v_{\max} = 3,000 \text{ km s}^{-1}$  and  $d = 4.8 \text{ kpc}$ , is shown in Figure 4. The best fit ejected mass is  $M_{\text{ej}} = 2.2 \times 10^{-4}$ , the ejection time  $t_0$  is 96 days, the electron temperature of the ejecta is  $T_e = 67,000 \text{ K}$ , and  $v_{\min}/v_{\max} = 0.2$ . Not only is this model consistent with the non-detections at early times, it provides a better fit to data at late times than the model in Figure 3, reproducing the steep decline observed in the multi-frequency light curve. The relatively high electron temperature found by the model fit is required to account for both the high peak flux densities and the observed rate of transition to an optically thin spectrum.

The fit to the data is shown in more detail in Figure 5, which plots the light curve at each frequency in separate panels. The model described above is over-plotted as a red line in each panel; it is an excellent fit to the light curves at high frequency ( $\gtrsim 13 \text{ GHz}$ ). However, at lower frequencies the model and the observed light curves diverge, with the measured flux densities rising and declining earlier than the best fit model predicts. Although the formal best-fit delay time is 96 days, our detection of optically thick emission on Day 66 that brightened in subsequent observations suggest that the actual delay time is probably closer to 50 days. The more gradual rise observed in the data, and the discrepancies between low and high frequencies, suggest that our simple model fails to include all the important physics during the earliest stages of mass ejection (see Section 5.3 for more discussion). Discrepancies between the data and the model during the light curve decline might be explained by non-isothermal ejecta, which likely exhibit a radial temperature gradient. Modeling of non-isothermal ejecta is outside the scope of this paper, but has been required in the past to explain the radio light curve of the nova V1974 Cyg (Hjellming 1996).

#### 4.2. Allowed ranges of the ejecta mass and electron temperature

There are significant degeneracies between the four fundamental parameters of the model ( $M_{\text{ej}}$ ,  $v_{\max}$ ,  $T_e$ ; and  $d$ ), as illustrated in Figure 6. Some of these parameters are poorly constrained by the data, for example  $v_{\max}$ , the maximum velocity of the ejecta. Although we take the value  $3000 \text{ km s}^{-1}$  reported by Osborne et al. (2011) as our fiducial value, a range of velocities have been reported in T Pyx during outburst (see e.g. Catchpole 1969). Similarly, although we favor the distance of  $4.8 \pm 0.5 \text{ kpc}$  found using light echos from the nebular remnant observed with HST (Sokoloski et al. 2012), distance estimates in the literature range from  $2.5 \text{ kpc}$  to  $>5 \text{ kpc}$ . In order to understand the range of allowed ejected masses associated with these uncertainties, we explored a plausible parameter space of ejecta velocity and distance; for each combination we obtained the best-fit ejected mass and electron temperature, fitting to all frequencies simultaneously. The results are shown in Figure 6.

A change in the distance simply moves the model light curves up and down in brightness, but it influences the derived  $M_{\text{ej}}$ , because more massive ejecta will have higher peak flux densities. Therefore, if T Pyx is located at a smaller distance, we find a smaller ejecta mass from our radio light curves (top panel of Figure 6). However, a smaller ejecta mass will also become optically thin more quickly because the density in the shell is lower. The electron temperature covaries with ejecta mass because higher temperatures make the ejecta brighter while they are optically thick, but also lead to them becoming optically thin faster. Therefore,  $M_{\text{ej}}$  and  $T_e$  are somewhat inversely related in then model fits, as seen by comparing the two panels in Figure 6. Finally, the expansion velocity essentially acts as a “stretch” parameter in the time dimension, with slower values of  $v_{\max}$  producing slower



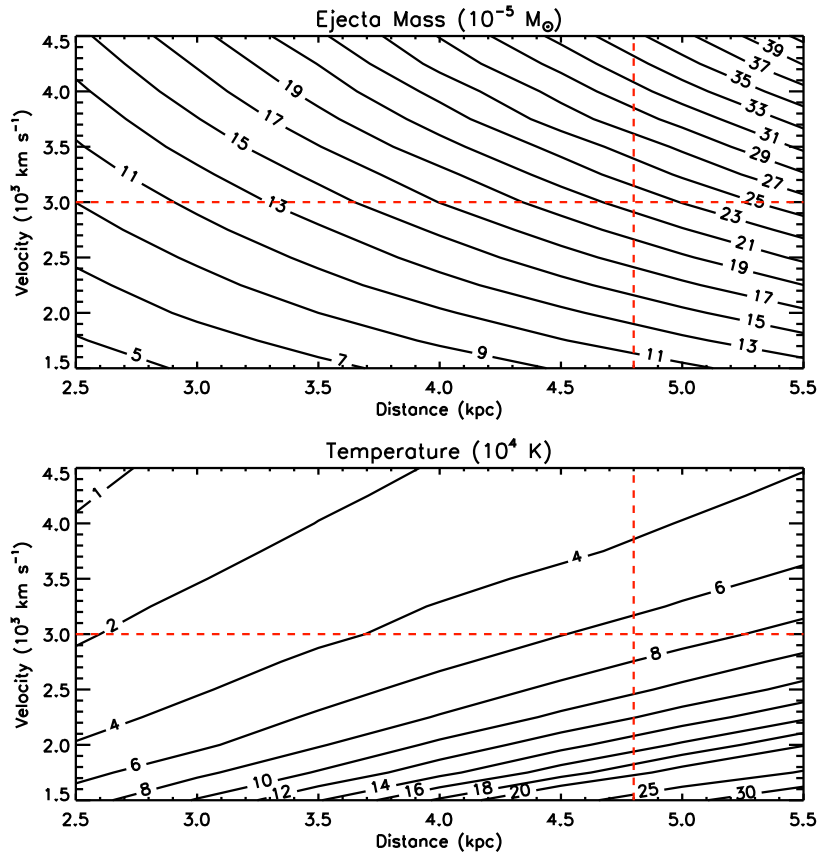


**Figure 6.** Illustration of the degeneracies in our model fit to the radio light curves of T Pyx. The derived values of ejecta mass ( $M_{\text{ej}}$ ; top panel) and electron temperature ( $T_e$ ; lower panel) depend on assumed values for the distance to T Pyx and the maximum expansion velocity in the nova outburst. Throughout this paper, we assume  $d = 4.8$  kpc and  $v_{\text{max}} = 3,000 \text{ km s}^{-1}$ , as constrained by optical observations; these parameters are marked as dashed red lines.

light curve evolution at all stages.

By applying observational constraints on two of the four fundamental parameters with measurements, we can find non-degenerate fits to the other two; for the remainder of our discussion we consider  $v_{\text{max}}$  and  $d$  to be constrained by optical spectroscopy and light echo imaging with the *HST* (Osborne et al. 2011, Sokoloski et al. 2012, in preparation). We find that the ejected mass is in the range  $1.2\text{--}3.3 \times 10^{-4} M_{\odot}$  allowing for the 0.5 kpc uncertainty on the light echo-derived distance and assuming the ejecta velocity is in the range  $2000\text{--}4000 \text{ km s}^{-1}$ . The best fit models for all parameter combinations have significant delays in the ejection time relative to the optical discovery discovery, showing that this result is driven primarily by the early non-detections of the source, and is independent of the choice of  $v_{\text{max}}$  or  $d$ . The thickness of the shell,  $v_{\text{min}}/v_{\text{max}}$ , is largely determined by how flat-topped the radio light curve is, and is also independent of the assumed values of  $v_{\text{max}}$  or  $d$ .

#### 4.3. Modeling of Clumpy Ejecta

In the simple modeling applied thus far, we assumed that the ejecta are smoothly distributed with a volume filling factor of unity. However, there are indications from both optical spectroscopy during nova outbursts and imaging of nova remnants that ejecta are often clumpy, with filling factors in the range  $f = 10^{-5} - 10^{-1}$  (e.g., Williams 1994;

Andreä et al. 1994; Saizar & Ferland 1994; Mason et al. 2005; Ederoclite et al. 2006; Shara et al. 2012). T Pyx itself shows significant evidence for clumping in its older ejecta, as the surrounding  $\text{H}\alpha + [\text{N II}]$  nebula has been resolved into a ring of knots by *HST* (Shara et al. 1997; Schaefer et al. 2010).

An observed radio light curve can be produced by clumpy ejecta with relatively lower mass and electron temperature than is required for homogeneous ejecta. We can adapt our simple model of radio emission from novae to account for clumping if we assume that a single volume filling factor ( $f$ ) can describe the ejecta at all times and radii, and that the material between clumps is of zero density. We also continue to assume that the ejecta are isothermal. In this case, clumping simply increases the radio luminosity by a constant factor over the uniform-density case, with no changes to the time evolution or radio spectrum (Abbott et al. 1981; Nugis et al. 1998; Heywood 2004). The radio flux density from clumped ejecta is boosted by a factor:

$$S_{\nu, \text{clump}} = \left(\frac{1}{f}\right)^{2/3} S_{\nu, \text{uniform}}. \quad (1)$$

This trend is illustrated in Figure 7, where we hold  $d$  and  $v_{\text{max}}$  fixed and plot how best-fit ejecta mass and electron temperature vary with assumed values for  $f$ .

However, if the ejecta in the model are too clumpy, un-

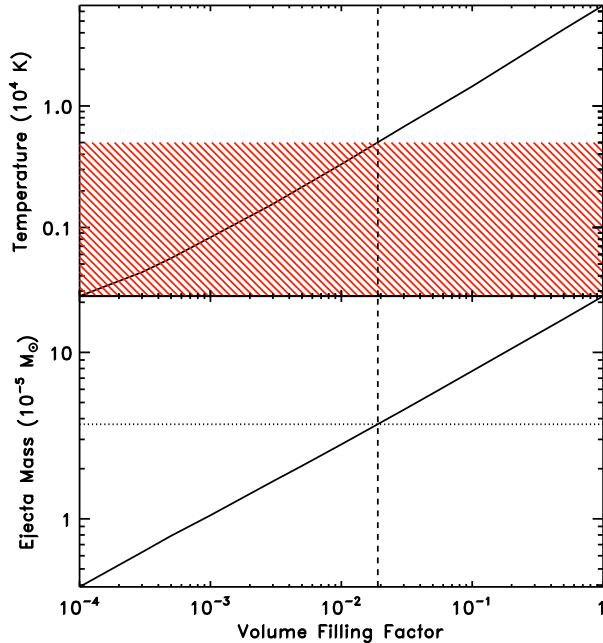


**Figure 7.** Best-fit electron temperatures (upper panel) and ejected mass (lower panel) for clumpy ejecta models with a range of volume filling factors, assuming  $d = 4.8$  kpc and  $v_{\max} = 3,000$  km s $^{-1}$ . The red hatched region in the top panel can be excluded because the electron temperatures are  $< 5,000$  K, i.e. too low for hydrogen to be ionized. The vertical dashed line therefore represents the minimum filling factor allowable ( $f = 0.02$ ). The horizontal dotted line in the bottom panel marks the ejecta mass that corresponds to this minimum filling factor,  $M_{\text{ej}} = 3.7 \times 10^{-5} M_{\odot}$ .

physically low temperatures are required to describe the light curve,  $T_e < 5,000$  K. At such low temperatures, hydrogen would not be ionized and no free-free radio flux would be emitted. We can therefore exclude the red area of parameter space in Figure 7 and place limits on the volume filling factor in T Pyx,  $f \gtrsim 0.02$ . This also allows us to place a lower limit on the ejecta mass in T Pyx of  $M_{\text{ej}} \gtrsim 3.7 \times 10^{-5} M_{\odot}$  (bottom panel of Figure 7). Accounting for the factor of  $\sim 2$  uncertainty introduced by the errors on the distance and ejecta velocity, this lower limit can be reduced to  $\sim 2 \times 10^{-5} M_{\odot}$ . We therefore conclude that the ejecta in T Pyx had a total mass in the range  $M_{\text{ej}} = (2 - 33) \times 10^{-5} M_{\odot}$ , spanning the parameter space from maximally clumpy to uniform density.

## 5. DISCUSSION

### 5.1. Alternative scenarios for producing radio emission in T Pyx

We assert in the previous section that the radio light curve is the product of material ejected during the 2011 nova outburst. In this section we show that other origins for the radio light curve can be confidently ruled out.

Given the extended nebular remnant around T Pyx visible in H $\alpha$ + [N II], it is conceivable that the radio emission could originate from this spatially-extended material, as the radiation associated with the outburst interacts with (and presumably ionizes) the remnant. Indeed, the timescales on which we see the radio emission develop are appropriate. Based on the *HST* imaging presented in Schaefer et al. (2010), the majority of clumps in the rem-

nant are located at distances between 2.3 and 5.5 arcsec from the central source. Placing T Pyx at 4.8 kpc, these angles correspond to physical distances of  $1.6 - 3.9 \times 10^{17}$  cm from the central system. The light crossing times to reach the inner and outer extents of the shell are therefore 62 and 149 days, respectively—corresponding roughly to the time we see the radio light curve rise and then fade.

However, the H $\alpha$  luminosities observed during the outburst from the extended remnant are much too low for the photoionized gas in the nebula to have produced the high observed radio flux density. An *HST* observation of T Pyx on 2011 September 25 (Day 164) using the F 656N filter yields an integrated H $\alpha$  flux for all knots beyond 3.5 arcsec of  $\sim 4 \times 10^{-17}$  erg s $^{-1}$  cm $^{-2}$  (A. Crots, private communication). Correcting for an interstellar E(B-V) of 0.49 using the extinction law of Fitzpatrick (1999), and using the conversion relation between H $\alpha$  and 5 GHz fluxes expected for a  $10^4$  K plasma given in Caplan & Deharveng (1986), we find that the observed H $\alpha$  flux implies a radio flux density at 5 GHz from the extended remnant of  $\sim 0.1 \mu\text{Jy}$ —five orders of magnitude lower than observed. Moreover, we never resolve the radio source associated with T Pyx, despite the fact that the VLA was in its relatively extended A- and B-configurations around light curve maximum. A nebula with a diameter of a few arcseconds would have been thoroughly sampled with  $\gtrsim 10$  synthesized beams across it at our higher observing frequencies, but T Pyx was consistent with a point-like distribution in all observations.

Another alternative scenario is that the radio emission originates in a dense medium in the immediate vicinity of the central binary. For example, Chomiuk et al. (2012) showed that the radio emission in the recent nova V407 Cyg originated primarily in the dense wind of the Mira giant companion in that system. During the period where stable nuclear burning took place on the white dwarf’s surface, the circumbinary medium was illuminated and ionized, and the radio flux density from this material increased. Could a similar mechanism be at play in T Pyx? Long-term optical light curves of T Pyx show a change in the orbital period with time, consistent with mass loss rate from the companion star as high as  $5 \times 10^{-7} M_{\odot} \text{ yr}^{-1}$  (Patterson et al. 1998; Uthas et al. 2010; Schaefer et al. 2011). If mass transfer in the system is even mildly non-conservative, then a significant amount of material could be lost into the circumbinary environment, which might emit in the radio once it is ionized by the nova outburst.

However, radio emission from this circumbinary material should emit in a manner similar to a stellar wind (see discussion in Chomiuk et al. 2012) and therefore exhibit a partially optically thin spectrum with  $\alpha \approx 0.6$ . The spectrum we observe during the rise is more consistent with a completely optically-thick body ( $\alpha \approx 1.8$ ), and the early increase in flux density implies that this body is expanding. In addition, if the circumbinary medium is in the immediate vicinity of the white dwarf, it would be difficult to account for the delay of  $\gtrsim 50$  days between the optical rise and the radio rise. Therefore, it is unlikely that T Pyx’s radio light curve is the result of ionization or interaction in a pre-existing circumbinary medium.

Given these factors, and the relatively good match be-



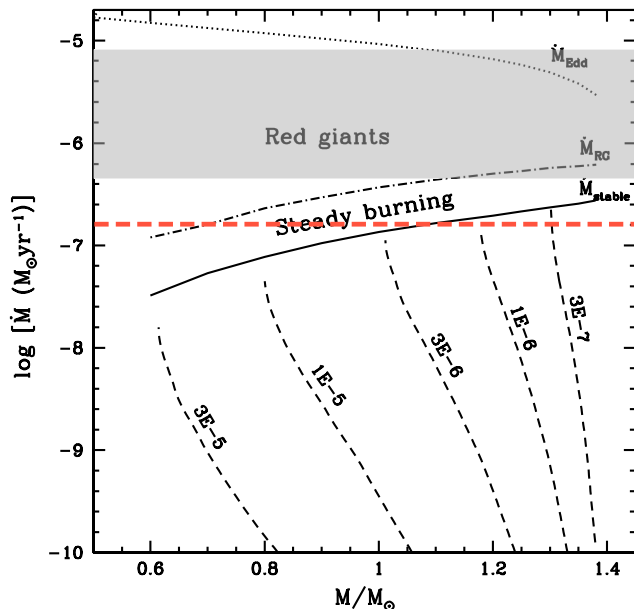


**Figure 8.** Figure 4 from Nomoto et al. (2007), plotting accretion rate against white dwarf mass and showing different regimes of accretion. Our estimated range of accretion rates in T Pyx is over-plotted as a grey shaded region, assuming that the entirety of  $M_{\text{ej}}$  was accreted since 1966. If instead we eject three times more mass than was accreted since 1966,  $\dot{M}$  could be as low as the dashed red line. At low accretion rates (below the solid line), the accreted material occasionally undergoes thermonuclear runaway in a nova outburst; estimated ejecta masses are marked with dashed lines. Intermediate accretion rates between the solid and dot-dashed result in steady nuclear burning of hydrogen on the white dwarf surface. High accretion rates above the dot-dashed line lead to unstable configuration wherein the accreted envelope expands in a “red giant”-like configuration.

tween the multi-frequency light curves and the simple model of expanding thermal ejecta presented in Section 4, we conclude that the expanding nova ejecta are the most likely origin of the radio emission.

### 5.2. Implications of a massive ejection event in T Pyx

The ejected masses derived from our model fits to the radio light curve are large, ranging from  $2 \times 10^{-5} M_{\odot}$  for clumped ejecta, to  $3.3 \times 10^{-4} M_{\odot}$  for a shell with a smooth density distribution of the form  $n \propto r^{-2}$ . Despite some uncertainties in the geometry, density profile, and temperature evolution of the ejecta, the primary constraint on the ejecta mass is simply provided by the high flux density observed at light curve maximum. We note that Selvelli et al. (2008) estimated an ejecta mass in the range  $10^{-5}$ – $10^{-4}$  for the 1966 outburst based on the long duration of the optically thick phase in the optical light curve—the radio data presented here support that conclusion. This high ejected mass challenges commonly held assumptions about T Pyx and holds important implications for the global parameters of the system.

Since we know the recurrence time of T Pyx, we can estimate the accretion rate in the system. Assuming that all the material ejected in the 2011 outburst has been accreted since the 1966 outburst, the average accretion rate is simply given by  $\dot{M} = \frac{M_{\text{ej}}}{t_{\text{rec}}}$ . For a recurrence time  $t_{\text{rec}} = 44$  years, our estimated range of  $M_{\text{ej}}$  implies an

accretion rate in the range  $\dot{M} = 4.5 \times 10^{-7} - 7.5 \times 10^{-6} M_{\odot} \text{ yr}^{-1}$ . Theoretical studies of nova outbursts find that some novae eject as much as three times the accreted mass (Yaron et al. 2005), in which case the accretion rate could be up to a factor of  $\sim 3$  lower (i.e.  $1.5 \times 10^{-7} - 2.5 \times 10^{-6} M_{\odot} \text{ yr}^{-1}$ ).

Estimates of the accretion rate from observations imply accumulated masses since the 1966 outburst that are only just compatible with the very lowest ejecta masses we have derived from the radio data—and only if the nova outburst ejects more material than was previously accreted. Assuming  $E(B-V) = 0.49 \pm 0.17$  (Shore et al. 2011), and a distance to T Pyx of 4.8 kpc, the UV flux reported in Selvelli et al. (2008) is consistent with a mass accretion rate as high as  $\sim 10^{-7} M_{\odot} \text{ yr}^{-1}$ . Uthas et al. (2010) present a new determination of the orbital period of T Pyx based on 14 years of photometric data, and find highly significant evidence of a period slow down (confirming the earlier result of Patterson et al. (1998)) that implies mass loss from the companion star. They derive a mass loss rate of  $5 \times 10^{-7} M_{\odot} \text{ yr}^{-1}$  using their estimate of the mass ratio in the system, and note that this represents the upper limit to the mass accretion onto the white dwarf—the rate could be lower if mass transfer is non-conservative.

The range of accretion rates implied by our radio light curves is also uncomfortably high in light of theoretical expectations for the fate of accreted material on a white dwarf. According to studies of thermal stability on white dwarfs (e.g., Nomoto 1982; Nomoto et al. 2007), at low accretion rates ( $\dot{M} \lesssim 10^{-7} M_{\odot} \text{ yr}^{-1}$ ), accreted material collects on the white dwarf until a critical pressure  $P_{\text{crit}}$  is reached and a nova outburst is triggered (Figure 8). In a relatively narrow range of higher accretion rates ( $\dot{M} \approx [1 - 6] \times 10^{-7} M_{\odot} \text{ yr}^{-1}$ ), the white dwarf can stably fuse hydrogen in the accreted shell. Finally, at the highest accretion rates ( $\dot{M} \gtrsim 6 \times 10^{-7} M_{\odot} \text{ yr}^{-1}$ ), it is likely that mass transfer onto the white dwarf will be unstable, and the accreted material will puff up into an extended red-giant-like atmosphere, or be expelled from the white dwarf in an optically-thick accretion wind (Hachisu et al. 1999).

T Pyx produces novae despite experiencing an accretion rate that is  $\sim 1$ – $2$  orders of magnitude higher than predicted for nova-hosting white dwarfs. The accretion rates implied by our radio-derived ejecta masses and the recurrence time in T Pyx are so high that T Pyx was expected to have been in an unstable red-giant-like configuration during quiescence (grey bar in Figure 8). Even under the most conservative assumptions of the clumpiest, lowest-mass ejection allowed by our radio light curves, and an ejected mass that is three times larger than the accreted mass, the accretion rate is still high enough that the white dwarf would have at least been stably burning hydrogen on its surface in the standard theoretical picture. If the white dwarf had been in such a stable, hydrogen-burning configuration during quiescence, it would not have undergone a nova outburst in 2011. Indeed, a hypothesis that T Pyx might host a super-soft X-ray source (Patterson et al. 1998; Knigge et al. 2000) was over-turned by X-ray observations during quiescence, which showed no evidence for stable nuclear burning (Selvelli et al. 2008). In addition, there is no ev-

idence for a red-giant-like extended envelope or optically-thick wind during quiescence (Gilmozzi & Selvelli 2007; Selvelli et al. 2008). T Pyx may therefore present a significant challenge to the theory of accretion onto white dwarfs, and warrant a re-investigation of the parameter space laid out by Nomoto et al. (2007), as plotted in Figure 8. Our estimate for the average rate of mass transfer in T Pyx can only be brought into line with accretion theory if we allow the distance to be significantly lower than the  $4.8 \pm 0.5$  kpc assumed here, and let the filling factor and  $T_e$  of the ejecta to take on their minimum allowable values.

The large ejecta mass measured during the 2011 outburst of T Pyx implies that the white dwarf has a mass that is lower than usual for a recurrent nova. Thermonuclear runaways on the surface of accreting white dwarfs are triggered when the pressure in the accreted shell

$$P = \frac{GM_{\text{WD}}m_{\text{acc}}}{4\pi R_{\text{WD}}^4} \quad (2)$$

reaches  $P_{\text{crit}} \approx 10^{19}$  dyn cm $^{-2}$  (Fujimoto 1982; MacDonald 1983). Assuming that the ejected mass and the mass accreted between nova outbursts are essentially equivalent, and using the relationship between white dwarf mass and radius from Hamada & Salpeter (1961), we find that white dwarfs with masses between 0.65 and 1.1  $M_{\odot}$  reach  $P_{\text{crit}}$  with our estimated range of  $M_{\text{ej}}$ . If the nova ejected three times more mass than it accreted, the white dwarf mass could be as high as 1.2  $M_{\odot}$ . For higher mass white dwarfs, a nova outburst would have been triggered at a significantly lower accreted mass.

The results of detailed modeling of accretion-outburst cycles in novae confirm this basic reasoning. In the full grid of models presented by Yaron et al. (2005), only white dwarfs with masses  $< 1.25 M_{\odot}$  can ever accrete a shell of  $10^{-5} M_{\odot}$  or greater. Townsley & Bildsten (2004) note that high mass accretion rates, such as the one we have inferred in T Pyx, actually reduce the TNR trigger mass for a given white dwarf mass relative to low accretion rates by up to an order of magnitude. The mass estimates we have calculated using Equation 2 are therefore only upper limits to the white dwarf mass. Uthas et al. (2010) find a white dwarf mass of  $0.7 \pm 0.2 M_{\odot}$  based on time-resolved optical spectroscopy and assumptions about the density of the secondary. Although the derivation of white dwarf mass from a spectroscopic period depends on several uncertain assumptions, the data are compatible with a low-mass white dwarf. Higher white dwarf masses (generally 1.3  $M_{\odot}$ ) are quoted extensively in the literature for T Pyx, although this value appears to be based primarily on the expectation of a high-mass white dwarf in system with short nova recurrence time (e.g., Webbink et al. 1987). Our results present a significant challenge to this assumption.

### 5.3. A prolonged, multi-stage ejection in T Pyx

The radio evolution we have observed in T Pyx is not consistent with a single impulsive ejection of the bulk of material on day zero. In fact, there is evidence that mass ejection took place in at least two stages. Shore et al. (2011) derive an ejected mass from optical spectroscopy obtained on Days 1 and 9 of  $M_{\text{ej}} \approx 2 \times 10^{-5} f M_{\odot}$ , where  $f$  is the volume filling factor. This is incompatible with

our radio derived mass range, since inconsistent filling factors are required to bring the estimates into agreement. However, it is possible that these spectra trace only the earliest epoch of mass ejection. We note that the single 33 GHz detection of T Pyx with the VLA on Day 14 is consistent with optically thick emission, and therefore could originate in an ejected shell. The low flux density, and subsequent radio non-detections indicate that the mass associated with this ejection must be small, at most  $10^{-6} M_{\odot}$ . This is consistent with the estimate from Shore et al. (2011) if the filling factor is small,  $f \leq 0.1$ .

The bulk of the ejection of material in T Pyx did not happen until several months after optical discovery. As we outlined in Section 4.1, the late rise of the radio emission indicates that the primary mass ejection took place 50–100 Days after  $t_0$ . However, even allowing for a late ejection, the light curves deviate from the  $S_{\nu} \propto t^2$  rise expected from an optically thick shell expanding at constant velocity. The observed flux density increase between Days 66 and 194 cannot be reconciled with ejecta expanding at a constant velocity emitted around Day 66. In fact, the C-band light curve observed between Days 45 and 102 rise more as  $S_{\nu} \propto t^1$ , which may indicate a more gradual ejection of material, although the data are insufficient to draw a definitive conclusion.

Regardless of the exact details of the earliest stages of mass ejection traced by the main radio rise, it is clear that T Pyx experienced a significant delay in the ejection of the bulk of its accreted shell. This delay may provide an explanation for the optical evolution of T Pyx. As evidenced in the AAVSO optical light curve shown in Figure 1, T Pyx shows a dramatic plateau in optical brightness, and does not begin its optical decline phase until  $\sim 90$  days after the start of the outburst. The time of this transition in the optical light curve roughly coincides with the rise of the radio light curve, as expected for an optical photosphere that has been approximately constant in size for a few months, and suddenly begins to recede through the ejecta as they start expanding.

Other novae have shown similar plateaus around optical maximum, with the duration of the plateau widely varying between sources, from a few to hundreds of days (e.g., Kato & Hachisu 2011). The physical origin of these plateaus around maximum is unclear, although they generally last longer on slower novae. Friedjung (1992) noted that during the plateau in HR Del, the optical spectrum showed no evidence of an optically-thick wind as typically seen in other novae; it was in fact more consistent with an almost stationary atmosphere. The author proposed that the nova outburst in this system was initially not strong enough to eject the accreted envelope, and instead settled into a quasi-static configuration with little mass loss. No explanation was offered, however, for the transition to the subsequent phase of significant mass loss. The plateau around maximum in T Pyx could be interpreted in the same way, and indeed the late ejection implied by the radio light curves lends credence to the idea of a stable, quasi-hydrostatic phase in the early stages of outburst in T Pyx. If the nova had been losing significant amounts of mass at high velocities from the onset of outburst, we would have detected the source at higher radio flux densities during our early observations.

Hachisu & Kato (2004) concurred that plateaus

around optical maximum could be interpreted as a static phase of the outburst, with an inflated but stable white dwarf photosphere formed after the onset of the thermonuclear runaway. In later work (Kato & Hachisu 2011), the same authors proposed that the friction provided by the companion star interacting with the hydrostatic envelope could provide an additional source of energy, empowering the outburst to transition from a stable to a mass-losing configuration. Although we do not speculate as to whether orbital friction played a role in the observed late ejection in T Pyx, it is worth noting that Kato & Hachisu (2011) find that this mechanism should be most efficient in very short period binaries, like T Pyx, where the companion becomes deeply embedded in the nova envelope.

## 6. CONCLUSIONS

From our analysis of multi-frequency radio light curves obtained with the newly-upgraded VLA, we reach several conclusions that challenge some of the most fundamental and commonly-held beliefs about the T Pyx binary system.

1. The 2011 nova event in T Pyx expelled a large amount of mass, totaling  $[2 - 33] \times 10^{-5} M_{\odot}$ .
2. In order to have accreted sufficient material since 1966 to account for this large ejecta mass, the white dwarf in T Pyx must have been accreting material at a very high rate,  $\dot{M} \gtrsim 1.5 \times 10^{-7} M_{\odot} \text{ yr}^{-1}$ .
3. Such a high nova trigger mass implies that the white dwarf in T Pyx is not near the Chandrasekhar mass. Instead, it more likely has a mass of  $\lesssim 1 M_{\odot}$ .
4. The bulk of the mass was not ejected from the white dwarf until  $\sim 50$ – $100$  days after the optical discovery.

We are grateful to H. Uthas, M. Shara, J. Patterson, and S. Starrfield for illuminating discussions. We thank NRAO for the generous allocation of director's discretionary time that made this work possible. We are also grateful to the VLA commissioning team, including J. McMullin, J. Wrobel, E. Momjian, L. Sjouwerman, and G. van Moorsel, for their assistance in the acquisition of this data set. The National Radio Astronomy Observatory is a facility of the National Science Foundation operated under cooperative agreement by Associated Universities, Inc. L. Chomiuk and N. Roy are Jansky Fellows of the National Radio Astronomy Observatory. J. L. S. and J. W. acknowledge support from the National Science Foundation through award AST-1217778. Finally, we acknowledge with thanks the variable star observations from the AAVSO International Database contributed by observers worldwide and used in this research.

*Facilities:* AAVSO, Karl G. Jansky VLA

## REFERENCES

- Abbott, D. C., Biegging, J. H., & Churchwell, E. 1981, *ApJ*, 250, 645
- Andre , J., Drechsel, H., & Starrfield, S. 1994, *A&A*, 291, 869
- Caplan, J., & Deharveng, L. 1986, *A&A*, 155, 297
- Catchpole, R. M. 1969, *MNRAS*, 142, 119
- Chomiuk, L., Krauss, M. I., Rupen, M. P., et al. 2012, *ApJ*, in press
- Ederoclite, A., Mason, E., Della Valle, M., et al. 2006, *A&A*, 459, 875
- Fitzpatrick, E. L. 1999, *PASP*, 111, 63
- Friedjung, M. 1992, *A&A*, 262, 487
- Fujimoto, M. Y. 1982, *ApJ*, 257, 752
- Gehrz, R. D., Truran, J. W., Williams, R. E., & Starrfield, S. 1998, *PASP*, 110, 3
- Gilmozzi, R., & Selvelli, P. 2007, *A&A*, 461, 593
- Hachisu, I., & Kato, M. 2004, *ApJ*, 612, L57
- Hachisu, I., Kato, M., & Nomoto, K. 1999, *ApJ*, 522, 487
- Hamada, T., & Salpeter, E. E. 1961, *ApJ*, 134, 683
- Heywood, I. 2004, PhD thesis, University of Manchester
- Hjellming, R. M. 1996, in *ASP Conf. Ser.*, Vol. 93, *Radio Emission from the Stars and the Sun*, ed. A. R. Taylor & J. M. Paredes, 174
- Hjellming, R. M., Wade, C. M., Vandenberg, N. R., & Newell, R. T. 1979, *AJ*, 84, 1619
- Kato, M., & Hachisu, I. 2011, *ApJ*, 743, 157
- Knigge, C., Baraffe, I., & Patterson, J. 2011, *ApJS*, 194, 28
- Knigge, C., King, A. R., & Patterson, J. 2000, *A&A*, 364, L75
- MacDonald, J. 1983, *ApJ*, 267, 732
- Markwardt, C. B. 2009, in *Astronomical Data Analysis Software and Systems XVIII*, ed. D. A. Bohlender, D. Durand, & P. Dowler, Vol. 411, 251
- Mason, E., Della Valle, M., Gilmozzi, R., Lo Curto, G., & Williams, R. E. 2005, *A&A*, 435, 1031
- Nomoto, K. 1982, *ApJ*, 253, 798
- Nomoto, K., Saio, H., Kato, M., & Hachisu, I. 2007, *ApJ*, 663, 1269
- Nugis, T., Crowther, P. A., & Willis, A. J. 1998, *A&A*, 333, 956
- Osborne, J. P., Beardmore, A. P., Page, K. L., et al. 2011, *ATel*, 3549, 1
- Patterson, J., Kemp, J., Sharnbrook, A., et al. 1998, *PASP*, 110, 380
- Saizar, P., & Ferland, G. J. 1994, *ApJ*, 425, 755
- Schaefer, B. E. 2010, *ApJS*, 187, 275
- Schaefer, B. E., Landolt, A. U., Vogt, N., et al. 1992, *ApJS*, 81, 321
- Schaefer, B. E., Pagnotta, A., & Shara, M. M. 2010, *ApJ*, 708, 381
- Schaefer, B. E., Landolt, A. U., Linnolt, M., et al. 2011, *arXiv* 1109.0065
- Schatzman, E. 1949, *Annales d'Astrophysique*, 12, 281
- Sequist, E. R., & Bode, M. F. 2008, in *Classical Novae*, 2nd Edition. Cambridge Astrophysics Series, No. 43, Cambridge: Cambridge University Press, ed. M. F. Bode & A. Evans, 141
- Sequist, E. R., & Palimaka, J. 1977, *ApJ*, 217, 781
- Selvelli, P., Cassatella, A., Gilmozzi, R., & Gonz lez-Riestra, R. 2008, *A&A*, 492, 787
- Shara, M. M., Zurek, D., De Marco, O., et al. 2012, *AJ*, 143, 143
- Shara, M. M., Zurek, D. R., Williams, R. E., et al. 1997, *AJ*, 114, 258
- Shore, S. N., Augsteijn, T., Ederoclite, A., & Uthas, H. 2011, *A&A*, 533, L8
- Starrfield, S., Truran, J. W., Sparks, W. M., & Kutter, G. S. 1972, *ApJ*, 176, 169
- Townsend, D. M., & Bildsten, L. 2004, *ApJ*, 600, 390
- Uthas, H., Knigge, C., & Steeghs, D. 2010, *MNRAS*, 409, 237
- Waagan, E., Linnolt, M., Bolzoni, S., et al. 2011, *CBET*, 2700, 1
- Webbink, R. F., Livio, M., Truran, J. W., & Orio, M. 1987, *ApJ*, 314, 653
- Williams, R. E. 1982, *ApJ*, 261, 170
- , 1994, *ApJ*, 426, 279
- Yaron, O., Prialnik, D., Shara, M. M., & Kovetz, A. 2005, *ApJ*, 623, 398

**Table 1**  
VLA Observations of T Pyx

Date (UT)	$t - t_0^a$ (Days)	Epoch	Conf.	Freq (GHz)	$S_\nu$ (mJy)	Freq (GHz)	$S_\nu$ (mJy)	Freq (GHz)	$S_\nu$ (mJy)	Freq (GHz)	$S_\nu$ (mJy)
2011 Apr 22.0	8.0	1	B	5.9	$0.003 \pm 0.008$						
2011 Apr 22.2	8.2	1	B	33.1	$0.016 \pm 0.030$						
2011 Apr 30.9	16.9	2	B	5.9	$0.027 \pm 0.011$						
2011 May 1.1	17.1	2	B	33.1	$0.248 \pm 0.040$						
2011 May 15.5	31.5	3	BnA	1.6	$-0.040 \pm 0.031$	6.0	$0.022 \pm 0.006$	14.3	$0.028 \pm 0.017$		
2011 May 15.9	31.9	3	BnA	3.0	$0.000 \pm 0.035$	8.4	$0.017 \pm 0.018$	22.0	$0.038 \pm 0.049$	33.0	$-0.046 \pm 0.055$
2011 May 29.0	45.0	4	BnA	1.5 14.3	$0.134 \pm 0.068$ $0.026 \pm 0.019$	3.0 22.0	$0.015 \pm 0.034$ $0.021 \pm 0.031$	6.0 33.0	$0.005 \pm 0.010$ $0.011 \pm 0.030$	8.4	$0.032 \pm 0.017$
2011 Jun 1.0	48.0	5	BnA→A	33.1	$0.048 \pm 0.029$						
2011 Jun 19.9	66.9	6	A	5.0	$0.130 \pm 0.017$	7.0	$0.194 \pm 0.016$				
2011 Jul 24.8	101.8	7	A	1.6 7.0	$0.082 \pm 0.040$ $0.529 \pm 0.039$	2.5	$0.119 \pm 0.052$	3.5	$0.185 \pm 0.039$	5.0	$0.304 \pm 0.031$
2011 Aug 20.7	128.7	8	A	1.3 5.0 16.0	$0.146 \pm 0.058$ $1.128 \pm 0.061$ $6.932 \pm 0.715$	1.8 7.0 22.0	$0.190 \pm 0.066$ $1.885 \pm 0.097$ $11.38 \pm 1.17$	2.5 8.4 29.0	$0.318 \pm 0.056$ $2.809 \pm 0.141$ $18.82 \pm 1.91$	3.5 12.6 37.0	$0.581 \pm 0.065$ $4.832 \pm 0.500$ $23.28 \pm 2.36$
2011 Sep 17.6	156.6	9	A→D	12.6 37.0	$11.09 \pm 0.12$ $47.90 \pm 4.94$	16.0	$14.20 \pm 1.44$	23.7	$26.93 \pm 2.71$	29.0	$38.97 \pm 3.94$
2011 Sep 24.6	163.6	10	A→D	2.5 8.4	$0.800 \pm 0.126$ $6.738 \pm 0.338$	3.5	$1.350 \pm 0.098$	5.0	$3.014 \pm 0.161$	7.0	$5.157 \pm 0.260$
2011 Oct 25.5	194.5	11	D	1.3 5.0 23.7	$-0.763 \pm 0.210$ $3.816 \pm 0.196$ $26.27 \pm 2.63$	1.8 7.0 29.0	$0.631 \pm 0.210$ $6.106 \pm 0.308$ $30.97 \pm 3.10$	2.5 12.9 37.0	$1.421 \pm 0.139$ $14.09 \pm 1.41$ $34.68 \pm 3.47$	3.5 16.0	$1.716 \pm 0.127$ $18.60 \pm 1.86$
2011 Nov 10.5	210.5	12	D	1.3 5.0 23.7	$0.057 \pm 0.243$ $3.685 \pm 0.190$ $26.32 \pm 2.63$	1.8 7.0 29.0	$0.774 \pm 0.243$ $6.263 \pm 0.315$ $30.51 \pm 3.05$	2.5 12.6 37.0	$1.166 \pm 0.136$ $14.16 \pm 1.42$ $33.40 \pm 3.35$	3.5 16.0	$1.797 \pm 0.124$ $17.64 \pm 1.77$
2011 Dec 7.4	237.4	13	D	1.3 5.0 23.7	$0.699 \pm 0.277$ $4.270 \pm 0.219$ $18.14 \pm 1.82$	1.8 7.0 29.0	$0.445 \pm 0.167$ $6.594 \pm 0.332$ $18.87 \pm 1.89$	2.5 13.3 37.0	$1.567 \pm 0.121$ $12.41 \pm 1.25$ $19.80 \pm 1.99$	3.5 16.0	$2.307 \pm 0.128$ $14.37 \pm 1.44$
2012 Jan 5.4	266.4	14	DnC	1.3 5.0 23.7	$0.277 \pm 0.210$ $4.345 \pm 0.222$ $10.12 \pm 1.01$	1.8 7.0 29.0	$0.477 \pm 0.121$ $6.096 \pm 0.307$ $9.449 \pm 0.952$	2.5 13.3 37.0	$1.528 \pm 0.146$ $8.995 \pm 0.903$ $9.061 \pm 0.926$	3.5 16.0	$2.659 \pm 0.153$ $9.434 \pm 0.947$
2012 Feb 8.2	300.2	15	C	1.3 5.0 23.7	$1.000 \pm 0.153$ $3.802 \pm 0.193$ $5.155 \pm 0.519$	1.8 7.0 29.0	$1.441 \pm 0.161$ $4.685 \pm 0.236$ $5.045 \pm 0.511$	2.5 13.3 37.0	$1.876 \pm 0.137$ $5.596 \pm 0.561$ $4.385 \pm 0.454$	3.5 16.0	$2.580 \pm 0.143$ $5.739 \pm 0.575$
2012 Mar 10.1	331.1	16	C	2.5 13.3 37.0	$1.757 \pm 0.112$ $3.981 \pm 0.401$ $2.826 \pm 0.329$	3.5 16.0	$2.335 \pm 0.127$ $4.125 \pm 0.416$	5.0 23.7	$3.085 \pm 0.160$ $3.645 \pm 0.371$	7.0 29.0	$3.492 \pm 0.177$ $3.031 \pm 0.324$
2012 Mar 27.1	348.1	17	C	1.3	$0.529 \pm 0.176$	1.8	$0.927 \pm 0.125$				
2012 Jul 22.7	465.7	18	B	1.4 5.0	$0.600 \pm 0.133$ $0.867 \pm 0.075$	1.8 7.0	$0.592 \pm 0.098$ $0.812 \pm 0.074$	2.6	$0.764 \pm 0.104$	3.5	$0.689 \pm 0.070$
2012 Sep 07.6	512.6	19	BnA	1.4 5.0	$0.622 \pm 0.132$ $0.669 \pm 0.065$	1.7 7.0	$0.562 \pm 0.077$ $0.496 \pm 0.048$	2.6	$0.683 \pm 0.083$	3.5	$0.642 \pm 0.058$
2012 Sep 23.5	528.5	20	BnA	13.3 37.0	$0.757 \pm 0.096$ $0.464 \pm 0.182$	17.5	$0.682 \pm 0.104$	23.7	$0.866 \pm 0.214$	29.0	$0.483 \pm 0.151$

<sup>a</sup> Time since optical discovery of the nova event (2011 April 14; Waagan et al. 2011).